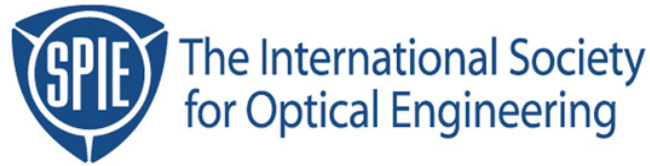


Copyright 1999 by the Society of Photo-Optical Instrumentation Engineers.



This paper was published in the proceedings of
Advances in Resist Technology and Processing XVI,
SPIE Vol. 3678, pp. 985-1000.

It is made available as an electronic reprint with permission of SPIE.

One print or electronic copy may be made for personal use only. Systematic or multiple reproduction, distribution to multiple locations via electronic or other means, duplication of any material in this paper for a fee or for commercial purposes, or modification of the content of the paper are prohibited.

Measurement of Parameters for Simulation of Deep UV Lithography Using a FT-IR Baking System

Atsushi Sekiguchi, Chris A. Mack*, Mariko Isono, Toshiharu Matsuzawa
Litho Tech Japan Corp., 2-6-6, Namiki, Kawaguchi, Saitama, 332-0034

**FINLE Technologies, Austin, TX 78746*

E-mail: jun@ltj.co.jp, chris_mack@finle.com

Abstract

A system for measurement of deprotection reaction parameters for use with chemically amplified (CA) resists was developed by incorporating baking equipment into a FT-IR spectrometer. Using this system, studies were conducted of a new model based on previous deprotection reaction models, but including the effects of deprotection reaction delay and the presence of a quencher. Used in these studies were a t-BOC/PHS resist for KrF excimer laser exposure, and a TBMA_{0.33}-IBMA_{0.33}-MMA_{0.33} copolymer resin resist for ArF excimer laser exposure. Deprotection reaction parameters for this model were measured for these two resists. The resulting parameters were then used with the PROLITH/2 lithography simulator for profile calculations, which were compared with SEM observation results. Though the simulation results were not in complete agreement with the SEM observations, general tendencies agreed quite well. This finding indicates that the present model may be reasonably applied to CA resists intended for KrF and ArF excimer laser exposure, and confirms the usefulness of the system described for deprotection reaction parameter measurement.

Keywords: Optical Lithography, Chemically Amplified Resist, Resist Kinetic, Lithography Simulation

1. Introduction

In the development of advanced lithographic technology, such as studies of new resist materials [1], resist processing variations [2], and phase-shifting mask methods [3], lithography simulation has proven to be a useful technique. In the post-exposure baking (PEB) of chemically amplified (CA) resists, diffusion of the acid generated by exposure and decomposition of protection groups (the deprotection reaction) occur simultaneously, and ultimately the concentration of the protection groups determines solubility in the developing fluid. Hence, in conducting simulations of lithography for CA resists, the simulation parameters involved in the deprotection reaction have a considerable effect on the simulation accuracy.

We have incorporated a bake plate in a FT-IR spectrometer for the *in situ* measurement by infrared spectroscopy of changes in reaction groups accompanying the deprotection reaction during PEB. Using this equipment, we have attempted to determine deprotection reaction simulation parameters for the cases of CA resists for use in KrF (248nm) and ArF (193nm) excimer laser exposure. Modeling was

based on the deprotection reaction analysis due to Petersen et al. [4] and Ohfuji et al. [5], extended to include deprotection reaction delay and base quenchers. Parameters obtained in this way were input to the PROLITH/2 lithography simulator [6] to simulate the profiles in a line-space pattern for KrF laser exposure at 0.25 μm feature sizes and ArF excimer laser exposure at 0.15 μm . The results were compared with SEM images of actual transfer patterns, and the validity of the system described was corroborated.

2. Hardware Configuration and Measurement Techniques

Figure 1 is an external view of the hardware. The FT-IR spectrometer was a model FTS-135 manufactured by Bio-Rad Corp. A 110 mm diameter bake plate with a 10 mm hole in the center was installed normal to the light path in the FT-IR measurement chamber. The wafer temperature uniformity was measured using a special instrumented wafer with five thermocouples. With the hotplate temperature set at 100°C, the wafer temperature was $98.0 \pm 0.2^\circ\text{C}$. No irregularities were observed in the temperature distribution over the 10 mm diameter hole. FT-IR measurements were performed in transmission mode. The IR measurement light penetrates the sample wafer (the measurement area is approximately 5 mm diameter), passes through the hole in the center of the bake plate, and enters the detector. The wafer is fixed in place by a vacuum clamp on a transport shuttle, and when the start button is pressed, is transported within 0.5 second to the bake plate. Proximity baking at a distance of approximately 0.2 mm was used. The *in situ* measurements are begun simultaneously with the initiation of baking. IR measurements were performed over the range 2000 to 500 cm^{-1} with a wavenumber resolution of 4 cm^{-1} . The number of cumulative measurement scans was set to one and sampling was performed every two seconds.

The IR signal was monitored at a wavelength properly chosen for each resist. Figure 2 shows the structural formulas of the resist materials used in these measurements and Figure 3 shows the protection group dissociation reactions thought to occur. The two resists used were: a) polyhydroxystyrene (PHS) with tertiary-butoxycarbonyl (t-BOC) and acetal as protecting groups, for use in KrF excimer laser exposure; and b) a tertiary copolymer resin (TBMA_{0.33}-IBMA_{0.33}-MMA_{0.33}) consisting of tertiary butyl methacrylate (TBMA), isobornyl methacrylate (IBMA), and methyl methacrylate (MMA) for ArF laser exposure. The photoacid generator used for both resists was triphenyl sulphonium triflate (TPS) and an aniline derivative was used as the quencher. The solvent was PGMEA in both cases. Figure 4 shows the infrared absorption spectrum for wavenumbers from 2000 to 500 cm^{-1} as a function of PEB time for these resists. We see that as the PEB time elapses (i.e., the deprotection reaction proceeds), there is a decrease in the strength of the absorption peak for the C-O (ether) bond between the protection groups and the resin, which occurs at 1150 cm^{-1} for the KrF resist and at 1144 cm^{-1} for the ArF resist. Deprotection reactions were then monitored by following the changes with PEB time in the infrared absorption spectrum at 1150 cm^{-1} for the KrF resist and at 1144 cm^{-1} for the ArF resist.

3. Calculation Model and Data Analysis

In order to analyze the kinetics of the deprotection reaction, the measured IR absorbance is converted into a normalized protection group concentration by comparing the change in absorbance after

a given bake time to the maximum possible change (i.e., from no deprotection to complete deprotection). This relative concentration of protected sites was then measured as a function of bake time for many exposure energies. By applying Petersen's and Ohfuji's deprotection reaction model (equation (1) below [4,5]) to this result, the best fit values for the deprotection reaction rate constant K_{dp} , the deprotection reaction order m , the PAG exposure rate constant C , and the acid lifetime τ , can be determined (see Figure 5).

$$[P] = \exp\left[-K_{dp}\{1 - \exp(-CE)\}^m \left\{1 - \exp\left(-\frac{mt}{\tau}\right)\right\} \frac{t}{m}\right] \quad (1)$$

where $[P]$ is the relative concentration of protected sites, E is the exposure energy, and t is the bake time. This model assumes a uniform exposure through the resist so that acid diffusion can be neglected. Note that if the resist is significantly absorbing this assumption could become quite inaccurate. Also, this model assumes that there is no room temperature deprotection so that $[P]$ always begins at 1.0 for $t = 0$. The acid lifetime τ is related to the bulk acid loss rate constant k_{loss} used by PROLITH/2 [6] by the expression

$$\tau = 1 / k_{loss} \quad (2)$$

We have adopted a new model equation, which adds to the previous model the effect of deprotection reaction initiation delay and the effect of acid capture by a quencher. The deprotection reaction delay effect occurs because several seconds (roughly 10 to 20 seconds) are required for the wafer to rise to the prescribed temperature when it is moved to the bake-plate and PEB is started in proximity mode. This delay in temperature increase appears as a delay in the onset of the deprotection reaction. This effect is readily studied through *in situ* measurements. This deprotection delay effect can be approximated by a simple delay time before the initiation of the deprotection reaction, T_d . Further, when a quencher exists in the resist, this quencher captures acid generated by exposure. This effect, in which the quencher causes a decrease in the acid concentration, is expressed by Q , the quencher concentration relative to the initial PAG concentration. Equation (3) is the expression for the new model.

$$[P] = \exp\left[-K_{dp}[H]^m \left\{1 - \exp\left(-\frac{m(t-T_d)}{\tau}\right)\right\} \frac{t}{m}\right] \quad (3)$$

where $[H] = 1 - \exp(-CE) - Q$

and where $[H]$ is the acid concentration relative to the initial PAG concentration.

4. Experimental Procedure and Results

The resist samples previously described were used in an attempt to confirm the accuracy of the model of the preceding section and to calculate their simulation parameters for PEB. The sample processing conditions were as follows.

KrF Resist:

Prebake: 90°C for 60 sec
Exposure: 0 – 100 mJ/cm²
PEB: 100°C – 130°C for 90 sec
PAG: 5 wt% of resin
Quencher: 0.1 wt% of resin ($Q = 0.02$)
Film thickness: 0.7 μm

ArF Resist:

Prebake: 120°C for 60 sec
Exposure: 0 – 100 mJ/cm²
PEB: 100°C – 130°C for 90 sec
PAG: 2 wt% of resin
Quencher: 0.1 wt% of resin ($Q = 0.05$)
Film thickness: 0.5 μm

For the KrF exposure, a simplified exposure system for experimental use, the UVES-2000, was used. For ArF exposure, the ArFES-3000 exposure system for photochemical analysis was used [7]. Figure 6 shows the relation between deprotection rate and PEB time at different PEB temperatures (100, 110, 120, 130°C) for the two resists. Here the exposure doses were 20 mJ/cm² for KrF exposure (E_{size} at 0.25 μm L/S for PEB at 100°C) and 20 mJ/cm² for ArF exposure (E_{size} at 0.15 μm L/S for PEB at 120°C). The wavy lines indicate the measured values, solid lines show the results of fitting to the equation. Good fits to the data were obtained in both cases.

5. Discussion of Results

5.1 Basic parameter extraction

In Figure 6 the data for the deprotection rate for different PEB temperatures are given for the KrF and ArF resists at one exposure. Simultaneous fitting of this data and data for other exposures to equation (3) allows all of the model parameters to be extracted at each PEB temperature. The exposure doses used were 0, 2, 4, 6, 8, 10, 20, 40, and 100mJ/cm² for both resists. Tables I and II show the deprotection reaction parameters for both resists and Figure 7 plots the resulting basic model parameters as a function of temperature. The exposure rate constant C , the quencher concentration Q , and the deprotection reaction order m do not vary appreciably with temperature, as expected. These parameters can be assumed to be constants for a given resist material. In addition, m is approximately 1.0 for both resists, indicating that a simple first order deprotection reaction is likely. The fitted quencher concentration matches the stoichiometric value quite well, indicating that the quencher used in these resists is not lost during the PEB and is 100% effective at quenching the acid. The variation of K_{dp} with temperature follows a classical Arrhenius behavior with an activation energy of 24.57 Kcal/mol ($\ln(Ar) = 29.82$) for the KrF resist and 34.47 Kcal/mol ($\ln(Ar) = 43.26$) for the ArF resist.

5.2 Effect of acid lifetime

The data in Figure 6 for the KrF resist indicates that as the PEB time increases, the deprotection curve changes in a linear fashion (on the logarithmic scale), but there is a large bend in the curve at a protection ratio of about 0.01. This suggests that when the protection ratio reaches a certain level, acid ceases to act as a catalyst and the deprotection reaction no longer proceeds. On the other hand, in the ArF resist the deprotection reaction curve is linear to the end, suggesting that in the range of practical PEB temperatures the acid lifetime in the deprotection reaction is sufficiently long.

Figure 8 shows the relation between PEB temperature and the extracted acid lifetime τ . For the KrF resist, as the PEB temperature increases we see that the acid lifetime is shortened. But in the ArF resist, the acid lifetime was found to be sufficiently long so that bulk acid loss is not contributing to the kinetics of deprotection. The two resists use the same PAG, thus, although the acid generated in the two is the same, differences in the polymer structure (including differences in the protecting groups) were found to give rise to differences in the acid lifetime. For the KrF resist, the variation of acid lifetime with temperature is well described by an Arrhenius behavior of k_{loss} with an activation energy of 15.21 Kcal/mol and $\ln(Ar) = 15.88$ (1/sec).

5.3 Effect of reaction initiation delay

On examining Figures 6 (a) and (b), it was found that the deprotection reaction tends to start slowly, then after a short time increase to its normal rate. For example, when PEB is at 110°C, the deprotection reaction in the ArF resist begins only after a holding time of about 20 seconds has elapsed. This suggests that if the resist has not heated sufficiently and the acid has not been activated, the deprotection reaction does not begin.

Figure 9 shows the relation between PEB temperature and the reaction delay time. In the ArF resist, as the PEB temperature increases the reaction delay is shortened. But in the KrF resist, the reaction delay time is unchanged regardless of the PEB temperature. More work is needed to clarify the reasons for this phenomenon.

6. Comparison of Experiment and Simulation

It was confirmed that the deprotection model adopted in this work is valid for KrF and ArF chemically amplified resists. The parameters obtained relating to the deprotection reaction were then input to the PROLITH/2 lithography modeling system, and simulations were conducted. In addition, KrF and ArF steppers were used to transfer patterns to resist, and SEM images of the results were compared with the simulation results. Exposure dose was calibrated between the steppers and the UVES-2000 and ArFES-3000 exposure tools using the resist dose to clear.

Conditions of KrF resist exposure:

Exposure wavelength: 248 nm
 NA: 0.57
 Coherence factor: 0.60
 Lines and spaces: 0.25 μ m
 Development: NDM-3 (2.38%), 60 sec
 BARC: 110 nm, $n=1.75$, $k=0.32$
 Substrate: Silicon

Conditions of ArF resist exposure:

Exposure wavelength: 193 nm
 NA: 0.60
 Coherence factor: 0.70
 Lines and spaces: 0.15 μ m
 Development: NDM-3 (2.38%), 60 sec
 BARC: 80 nm, $n=1.80$, $k=0.37$
 Substrate: Silicon

An ABC-Analyzer [8] was used to measure the Dill absorption parameters A and B. The RDA-790 Resist Development Analyzer [9] was used in measurements of development parameters. The DPC-

Software analysis system [10] was used to calculate the PAG diffusion constant D , development surface inhibition depth δ , and relative surface rate R_0 . All dissolution rate measurements used a 110°C, 90 second PEB. The simulation parameters were as follows.

KrF resist parameters:

Original Mack model
 $R_{\max} = 218 \text{ nm/s}$
 $R_{\min} = 0.13 \text{ nm/s}$
 $n = 6.38$
 $M_{\text{TH}} = 0.7$
 Acid diffusivity $D = 47.5 \text{ nm}^2/\text{s}$
 Inhibition depth $\delta = 83 \text{ nm}$
 Relative surface rate $R_0 = 0.64$
 Dill Parameter $A = -0.07 \text{ }\mu\text{m}^{-1}$
 Dill Parameter $B = 0.56 \text{ }\mu\text{m}^{-1}$

ArF resist parameters:

Original Mack model
 $R_{\max} = 198 \text{ nm/s}$
 $R_{\min} = 0.003 \text{ nm/s}$
 $n = 14.6$
 $M_{\text{TH}} = 0.7$
 Acid diffusivity $D = 50.3 \text{ nm}^2/\text{s}$
 Inhibition depth $\delta = 122 \text{ nm}$
 Relative surface rate $R_0 = 0.72$
 Dill Parameter $A = -0.66 \text{ }\mu\text{m}^{-1}$
 Dill Parameter $B = 1.29 \text{ }\mu\text{m}^{-1}$

Figure 10 (a) compares SEM images with simulation results for 0.25 μm line-space patterns obtained using KrF resist at different PEB temperatures. Though the exposure doses are not in complete agreement, the tendency for the sensitivity to rise with the PEB temperature is identical. In addition, the profiles yielded in simulations are in good agreement with the SEM observation results.

Figure 10 (b) similarly compares SEM images with simulation results for 0.15 μm line-space patterns obtained using ArF resist at different PEB temperatures. The SEM results indicate that at a PEB temperature of 100°C there is no resolution, and likewise the simulation results also show no resolution. At PEB temperatures of 110 and 120°C, both the SEM results and simulations indicate good resolution is obtained. At a PEB temperature of 130°C, however, there is some trailing off of the pattern. The profile obtained from simulations is not in complete agreement with this, but a similar tendency to trail off is seen. We see that the sensitivity increases with increasing PEB temperature as expected from the temperature dependence of K_{dp} .

Discrepancies between simulation and experiment could come from several sources. Development properties of the resist may vary somewhat with PEB conditions, but were only measured at one PEB condition. The diffusivity was assumed to be the same for all temperatures, although it most certainly should increase with increasing PEB temperature. Finally, different hotplates will exhibit different effective temperatures and delay times. No effort was made to calibrate the hotplate of the FT-IR to the hotplates used in the wafer processing fab.

7. Conclusion

Baking equipment was incorporated into a FT-IR spectrometer for measurement of deprotection reaction parameters. Using this system, a chemically amplified resist for KrF lithography (based on PHS using t-BOC) and a CA resist for ArF lithography (using a tertiary copolymer resin consisting of TBMA-IBMA-MMA) were used to corroborate the deprotection reaction modeling. Attempts were also made to

measure deprotection reaction parameters. The parameters obtained were input into the PROLITH/2 lithography simulation system to perform profile calculations, which were compared with actual SEM observation results. Though perfect agreement between simulations and SEM results was not obtained, the general trends observed in both were in good agreement. This result confirms the usefulness of the present measurement system for studying CA resists for use in deep-UV lithography.

Acknowledgements

In conducting this research, the authors received materials and cooperation in the SEM observations from Senior Researcher Uetani of the Fine Chemicals Research Laboratory of Sumitomo Chemical Co., Ltd. and from Dr. Tomita of the Photosensitive Materials Research Center of Toyo Gosei Co., Ltd., to whom we express our gratitude. We also wish to thank Dr. Ohfuji of Semiconductor Leading Edge Technologies, Inc. for useful advice concerning modeling of the deprotection reaction.

References

1. R. A. Fergason, J. M. Hutchinson, C. A. Spence, A. R. Neureuther, "Modeling and simulation of deep-ultraviolet acid hardening resist," *J. Vac. Sci. Technol.* B8 (6), pp.1423-1427, 1990.
2. C. A. Mack, M. J. Maslow, R. Carpio, and A. Sekiguchi, "Impact of Developer Temperature on Dissolution Behavior," *OCG Microlithography Seminar Interface '97*, (1997) pp. 203-212.
3. M. D. Levenson, N. S. Viswanathan, and R. A. Simpson, "Improving Resolution in Photolithography with a Phase-Shifting Mask," *IEEE Trans. Electron Devices*, ED-29 (1982) pp. 1828-1836.
4. J. S. Petersen, C. A. Mack, J. W. Thackeray, R. Sinta, T. H. Fedynyshyn, J. M. Mori, .D. Byers, and D. A. Miller, "Characterization and Modeling of a Positive Acting Chemically Amplified Resist," *Advances in Resist Technology and Processing XII, Proc.*, SPIE Vol. 2438, pp. 153-166, 1995.
5. T. Ohfuji, K. Nakano, K. Maeda, and E. Hasegawa, "Reaction Modeling of Chemically Amplified Resist for ArF Excimer", *J. Vac. Sci. Technol.*, B13 (6), pp. 3022-3025, 1995.
6. C. A. Mack, Inside PROLITH: A Comprehensive Guide to Optical Lithography Simulation, FINLE Technologies (Austin, TX: 1997).
7. A. Sekiguchi, M. Kadoi, T. Matsuzawa, Y. Minami, "Development of a System for Photochemical Analysis of ArF-Excimer Laser Processes," *Semiconductor World*, Vol. 6, June, pp. 25-30, 1997.
8. A. Sekiguchi, Y. Minami, T. Matsuzawa, T. Takezawa, H. Miyakawa, "Measuring System of A, B, and C Photoresist Parameters," *Electronics and Communication in Japan, Part 2*, Vol. 78, No. 5, pp. 21-30, 1997.
9. A. Sekiguchi, C. A. Mack, Y. Minami, T. Matsuzawa, "Resist Metrology for Lithography Simulation, Part 2 : Development Parameter Measurements," *Metrology, Inspection, and Process Control for Microlithography X, Proc.*, SPIE Vol. 2725, pp. 49-63, 1996.
10. A. Sekiguchi, M. Kadoi, T. Matsuzawa, Y. Minami, "Measuring System for Simulation Parameters of Chemical Amplification Resist System," *Electronics and Communication in Japan, Part 2*, Vol. J81, No. 6, pp. 542-549, 1998.

Table I. Results of parameter measurements for KrF resist.

Temp (°C)	K_{dp} (s^{-1})	m	C (cm^2/mJ)	τ (sec)	T_d (sec)	Q
100	0.034	1.01	0.053	95	16.2	0.020
110	0.104	1.08	0.055	58	15.0	0.021
120	0.160	1.14	0.058	51	15.0	0.019
130	0.456	1.08	0.053	18	15.0	0.020

Table II. Results of parameter measurements for ArF resist.

Temp (°C)	K_{dp} (s^{-1})	m	C (cm^2/mJ)	τ (sec)	T_d (sec)	Q
100	0.050	1.08	0.0044	930	30.0	0.050
110	0.098	1.00	0.0044	1080	22.0	0.050
120	0.385	1.20	0.0044	950	15.0	0.052
130	1.500	1.20	0.0040	970	11.0	0.049

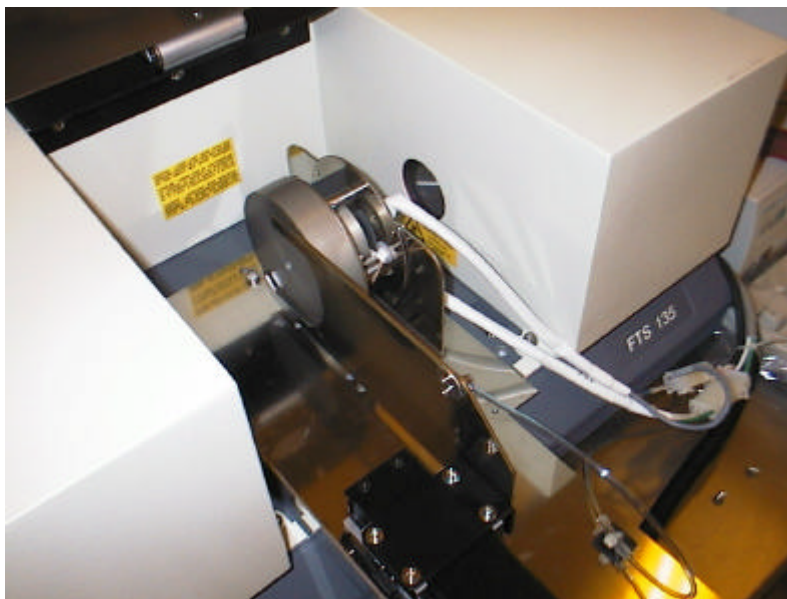


Fig.1. External view of the FT-IR measurement tool with wafer transport and *in situ* bake system.

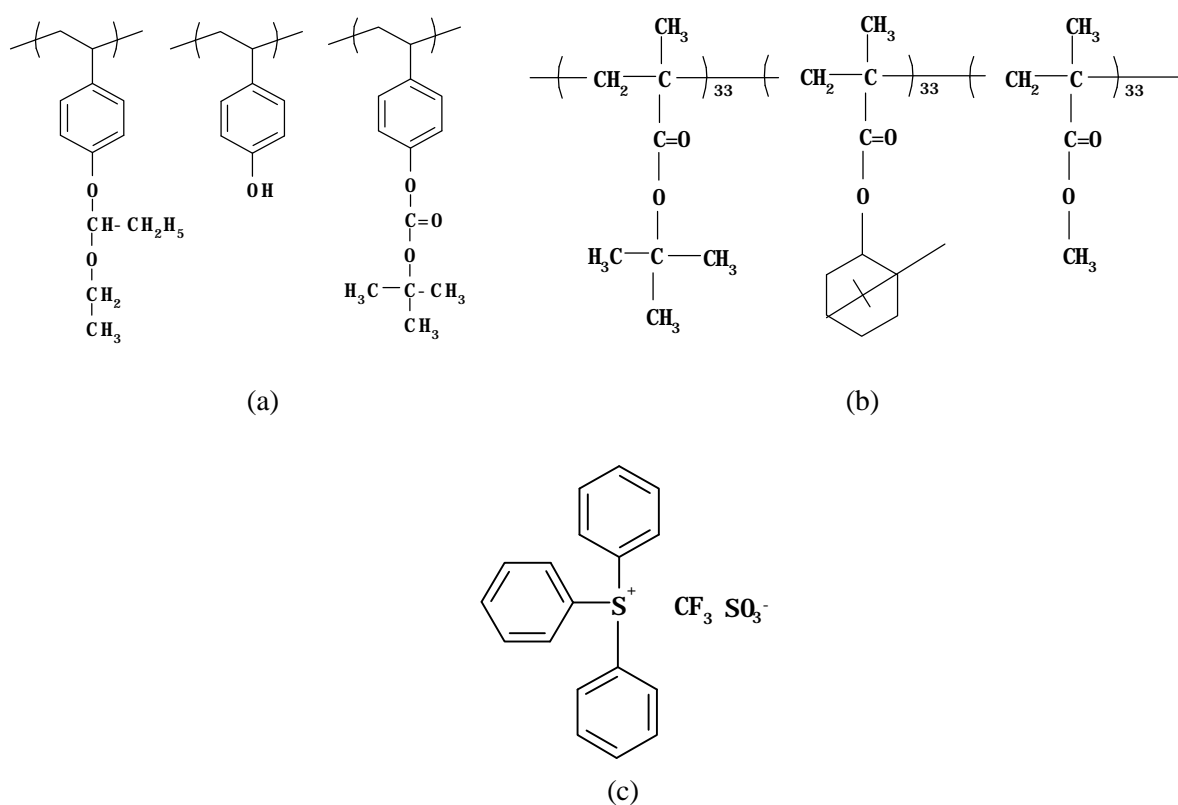
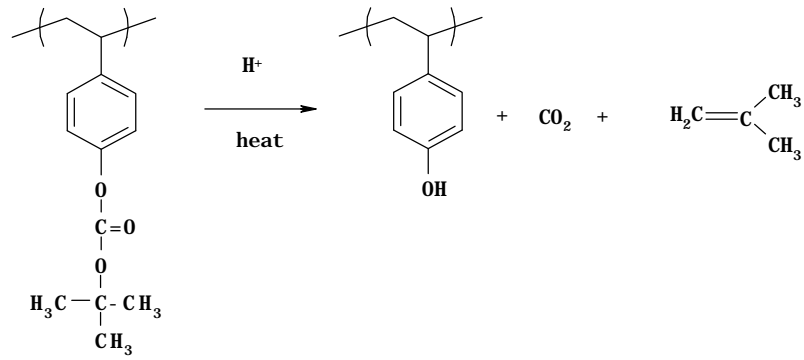
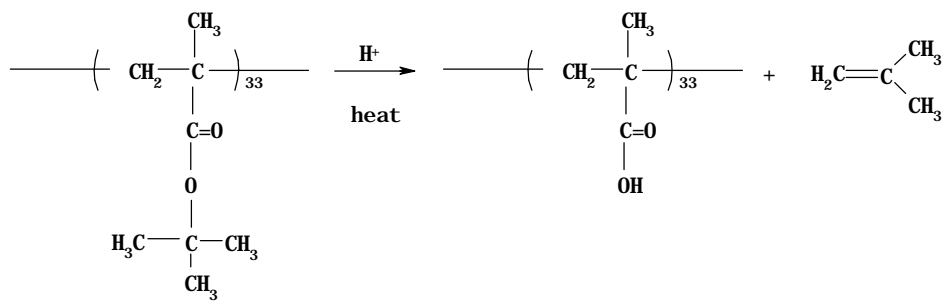


Fig.2. Chemical structure of (a) KrF CA resist (ethyl acetal-PHS-(t-BOC)), (b) ArF CA resist (TBMA_{0.33}-IBMA_{0.33}-MMA_{0.33}), and (c) the photoacid generator (TPS) used for both.

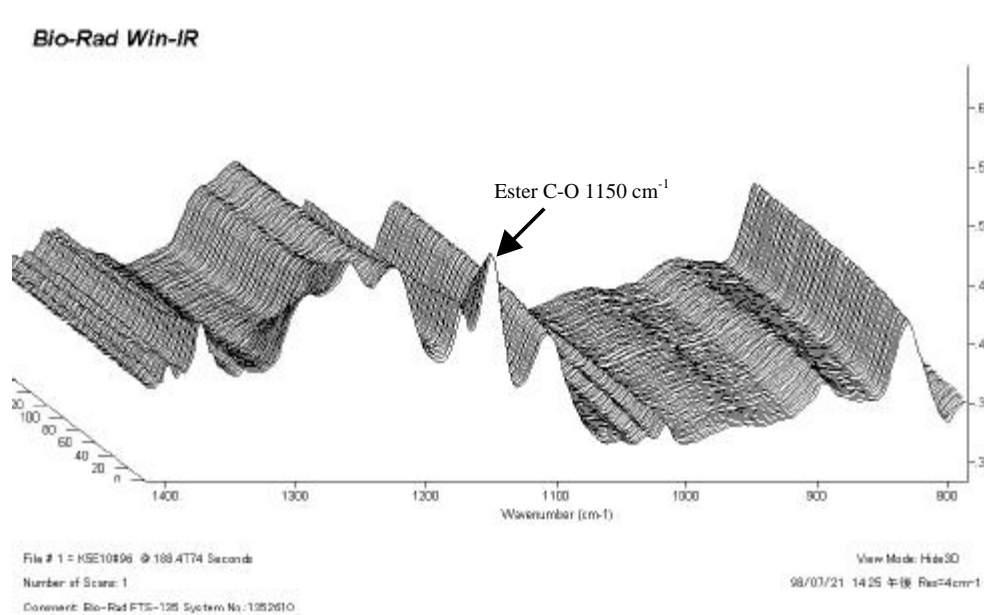


(a)

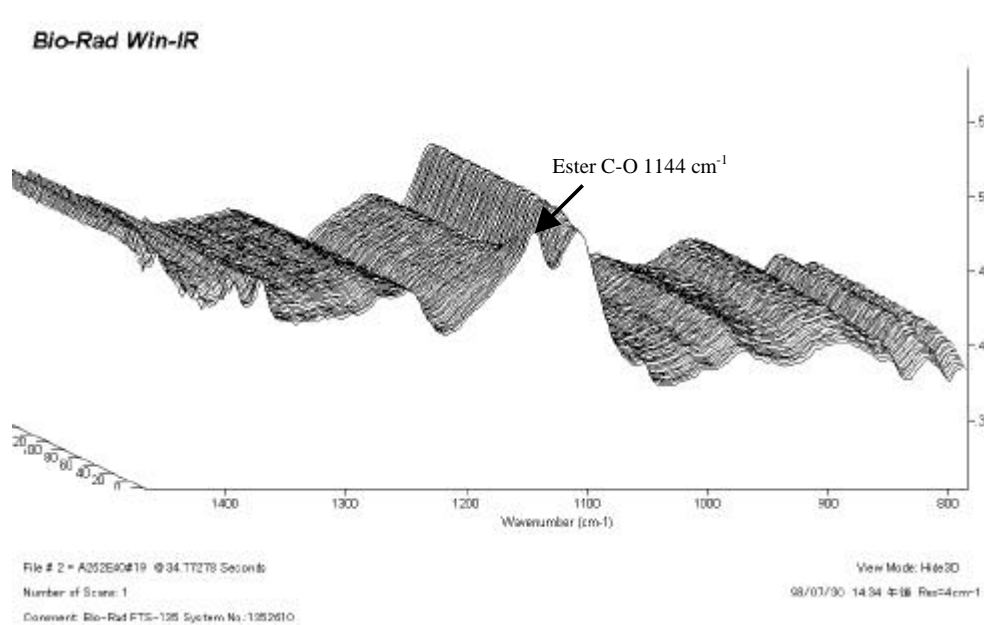


(b)

Fig.3. The expected deprotection reactions for (a) the KrF resist, and (b) the ArF resist.



(a)



(b)

Fig. 4. Typical FT-IR difference spectra showing deprotection reaction as a function of PEB time for (a) KrF resist, 110°C PEB temperature, exposed at 10mJ/cm², and (b) ArF resist, 110°C PEB temperature, exposed at 40mJ/cm².

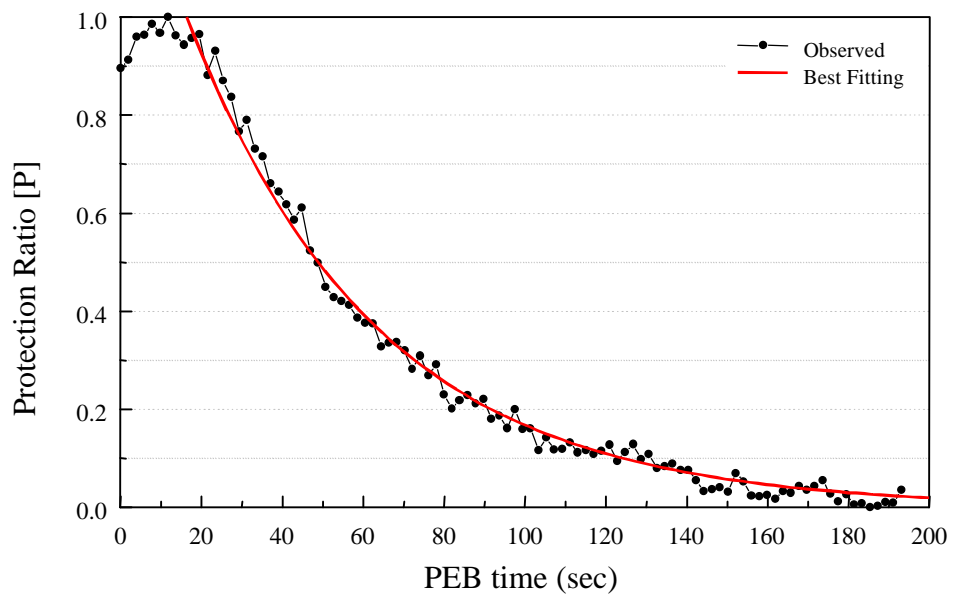


Fig. 5. A normalized protection ratio calculated from FT-IR spectra as a function of PEB time (ArF resist, 110°C PEB temperature, exposed at 40mJ/cm²).

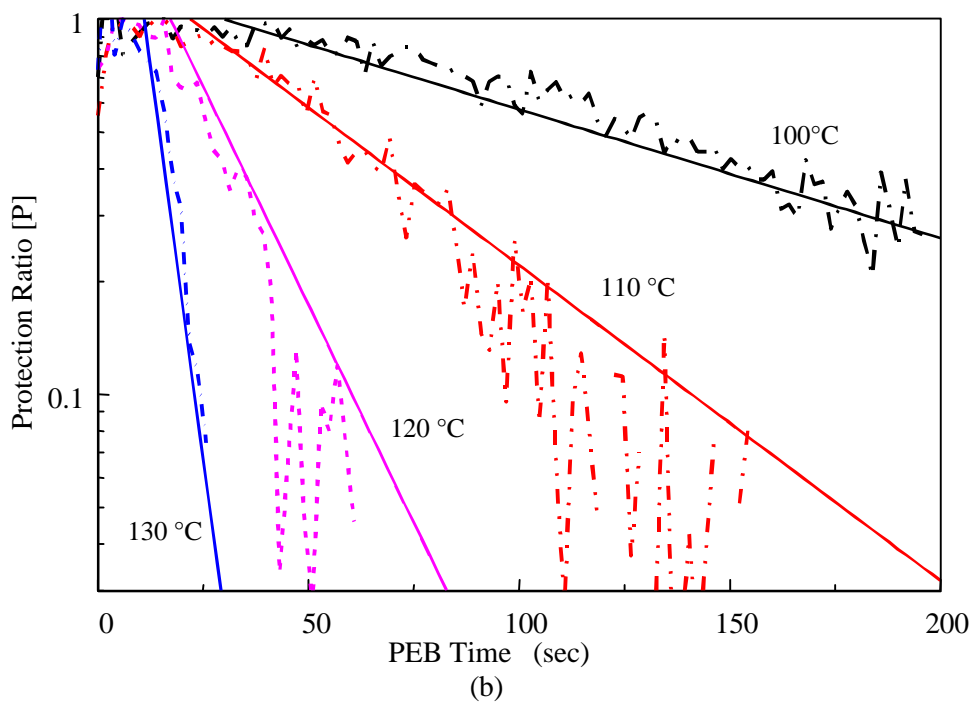
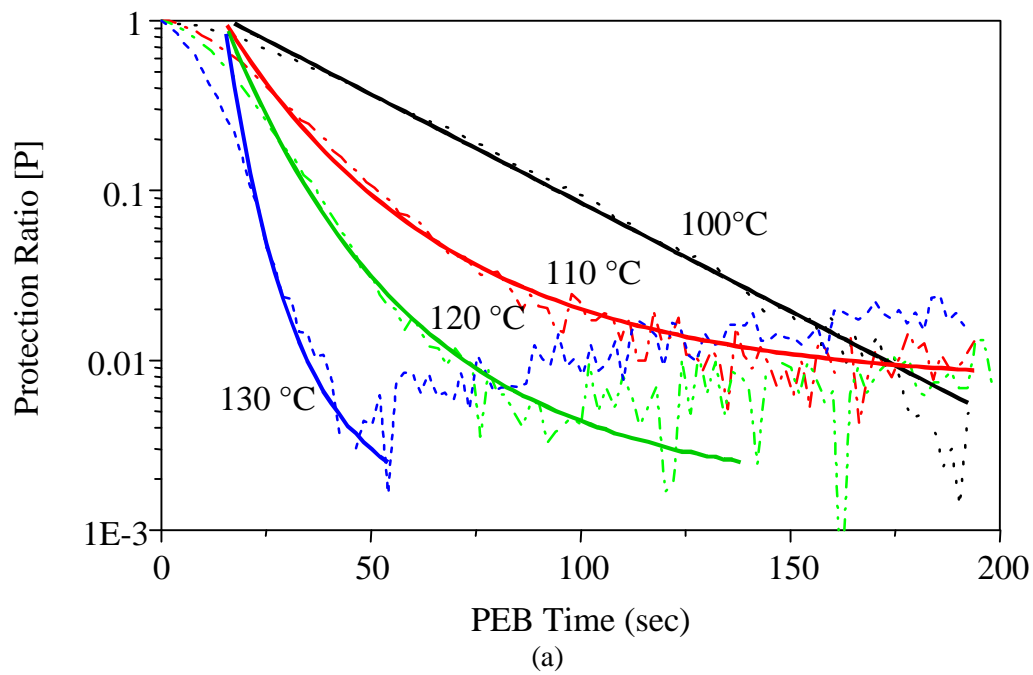


Fig. 6. Relationship between [P] and PEB time as a function of PEB temperature for (a) KrF resist, and (b) ArF resist. Exposure dose was 20 mJ/cm².

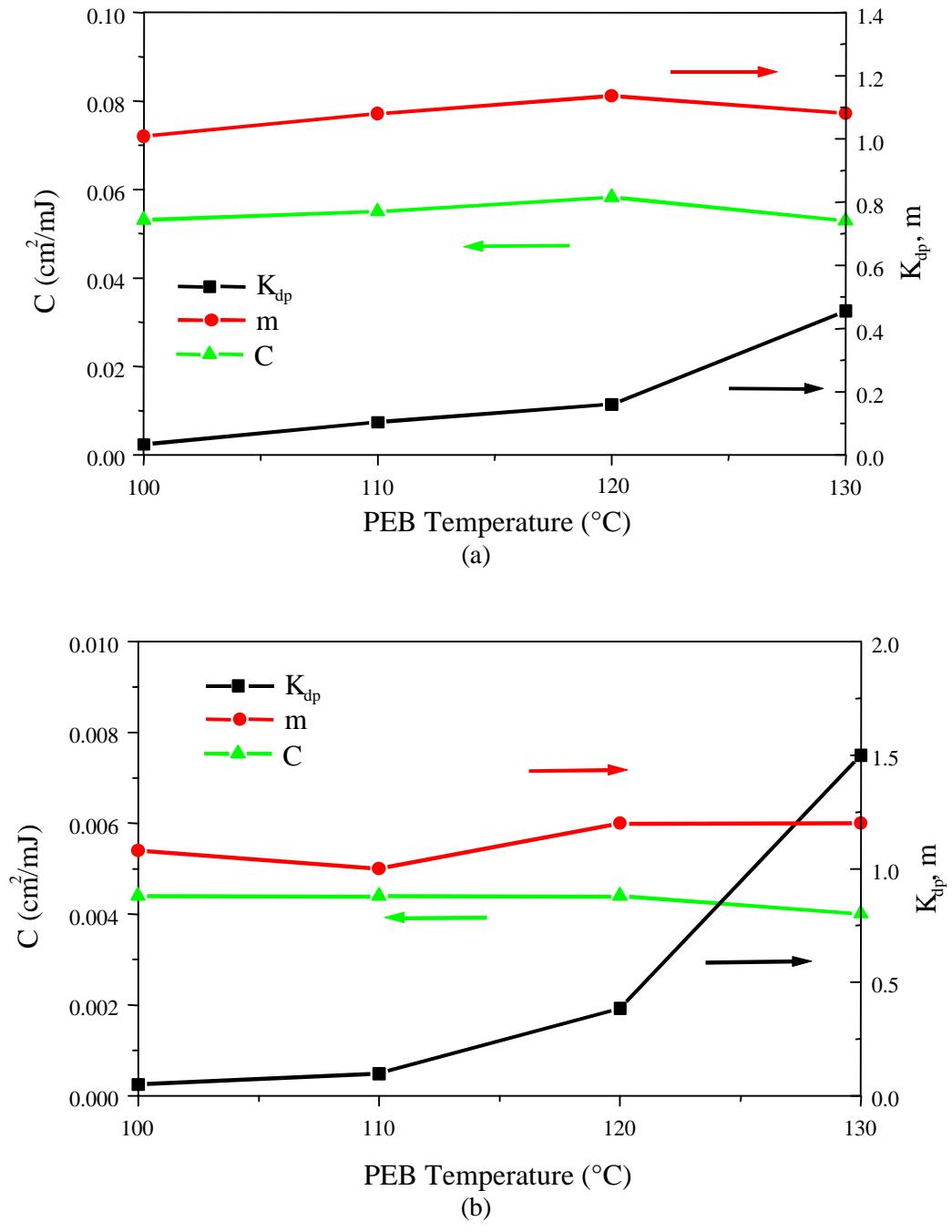


Fig. 7. Relationship between K_{dp} , C , m and PEB temperature for (a) KrF resist, and (b) ArF resist.

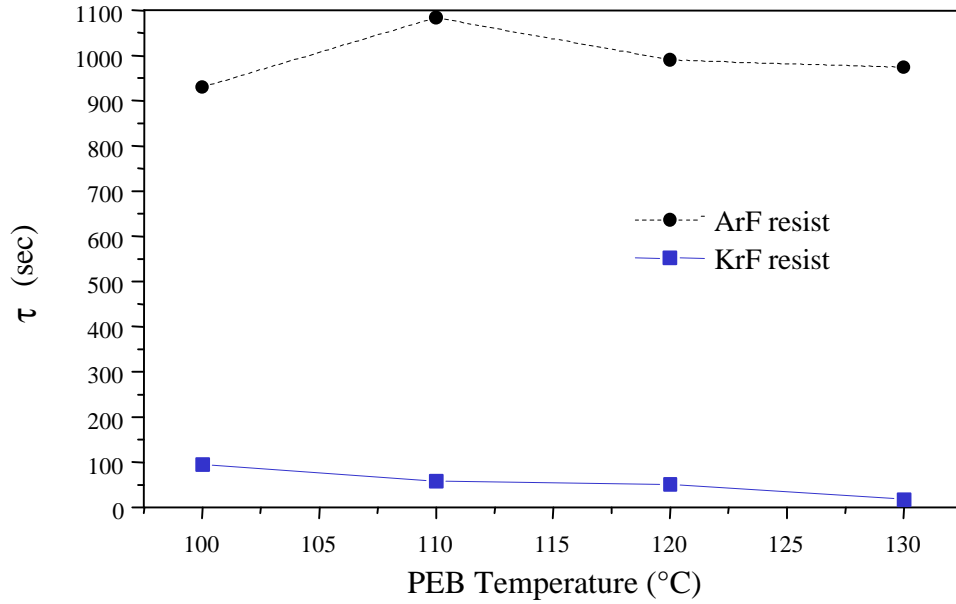


Fig. 8. Relationship between the acid lifetime τ and PEB temperature.

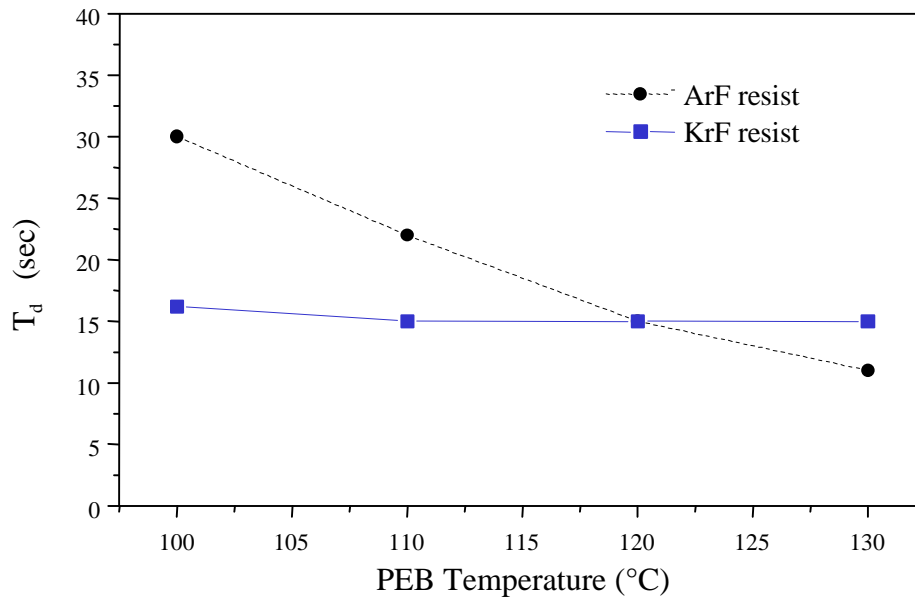
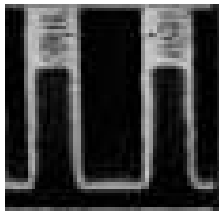
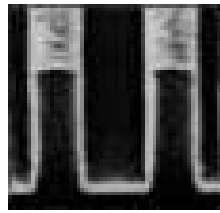
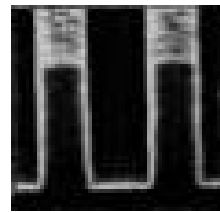
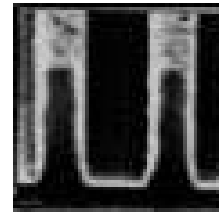
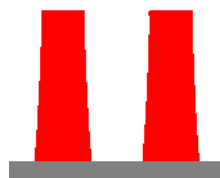
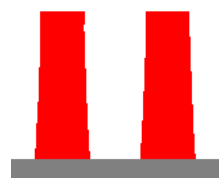
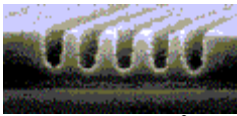
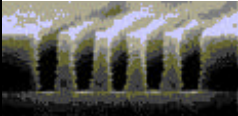
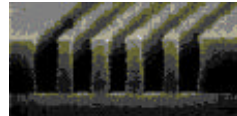
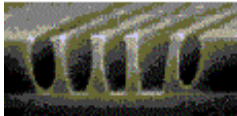


Fig. 9. Relationship between deprotection reaction delay time T_d and PEB temperature.

PEB	100°C	110°C	120°C	130°C
SEM	 22.50 mJ/cm ²	 7.00 mJ/cm ²	 3.25 mJ/cm ²	 1.50 mJ/cm ²
Simulation	 15.50 mJ/cm ²	 5.25 mJ/cm ²	 3.34 mJ/cm ²	 2.94 mJ/cm ²

(a)

PEB	100°C	110°C	120°C	130°C
SEM	 48.6mJ/cm ²	 33.9mJ/cm ²	 19.8mJ/cm ²	 14.8mJ/cm ²
Simulation	 50.0 mJ/cm ²	 33.1 mJ/cm ²	 22.5 mJ/cm ²	 20.0 mJ/cm ²

(b)

Fig. 10. Comparison between simulated profiles and SEM observation for (a) KrF resist ($L/S = 0.25\mu\text{m}$), and (b) ArF resist ($L/S = 0.15\mu\text{m}$) for different PEB temperatures at E_{size} .